Reza Sharif Razavian
Motion Research Group,
Systems Design Engineering,
University of Waterloo,
Waterloo, ON N2L 3G1, Canada
e-mail: rsharifr@uwaterloo.ca

Naser Mehrabi
Motion Research Group,
Systems Design Engineering,
University of Waterloo,
Waterloo, ON N2L 3G1, Canada
e-mail: nmehrabi@uwaterloo.ca

John McPhee
Fellow ASME
Professor
Motion Research Group,
Systems Design Engineering,
University of Waterloo,
Waterloo, ON N2L 3G1, Canada
e-mail: mcphee@uwaterloo.ca

A Neuronal Model of Central Pattern Generator to Account for Natural Motion Variation

We have developed a simple mathematical model of the human motor control system, which can generate periodic motions in a musculoskeletal arm. Our motor control model is based on the idea of a central pattern generator (CPG), in which a small population of neurons generates periodic limb motion. The CPG model produces the motion based on a simple descending command—the desired frequency of motion. Furthermore, the CPG model is implemented by a spiking neuron model; as a result of the stochasticity in the neuron activities, the motion exhibits a certain level of variation similar to real human motion. Finally, because of the simple structure of the CPG model, it can generate the sophisticated muscle excitation commands much faster than optimization-based methods.
[DOI: 10.1115/1.4031086]

1 Introduction

A significant portion of the human nervous system is devoted to sensorimotor integration. Human body motion is highly modulated by the high centers of the central nervous system (CNS) such as motor cortex and cerebellum; however, it is well-supported that some rhythmic motions (e.g., during locomotion) originate from the neural circuits within the spinal cord (see Refs. [1] and [2] for reviews). These specialized neural circuits, usually called a CPG, can generate rhythmic motoneuron activity without much need for extensive descending commands from higher parts of the CNS. Moreover, it has been shown that the generation of the rhythmic activity can occur without the presence of either the sensory feedback (deafferented) or descending command (spinalized/decerebrated preparations).

CPG-excited motion is particularly interesting in a motor control study from a theoretical perspective, as it can effectively address the redundancy in human musculature; the high-dimensional actuator space can be reduced to a low-dimensional control space, in which the motion can be modulated by only a small number of descending commands.

Previous mathematical studies of CPGs vary both in method and scale. The simplest network that can generate an oscillating motion is based on a half-center oscillator [3], in which two neurons reciprocally inhibit each other. By adding feedback loops [4], such a network is able to produce robust and controllable rhythmic signals. This simple model, however, is not able to generate sophisticated motoneuron patterns, as is observed in humans and animals.

To improve the half-center oscillator models, a layered structure is proposed in Refs. [5] and [6], where one layer is responsible for the generation of stable rhythms, while the second layer builds the bursting activities upon the rhythms. This architecture allows for including extra flexibility in the rhythm generation and in feedback modulation of motion.

In another approach, the wavelike body motions of a lamprey and salamander are generated by employing a set of interacting oscillators. In an early study [7], a series of neuronal oscillators were used to successfully simulate various lamprey locomotion speeds and turning patterns. This model was improved by including feedback modulation [8] and more realistic neuron models [9]. Similarly, CPG models including interconnected oscillators have been used to replicate swimming and trotting locomotion patterns in salamander simulations [10] and in a salamander robot [11]. In these salamander CPGs, the various locomotion patterns are created by increasing the controller input (similar to increasing the stimulation of the midbrain locomotor region). In a later study [12], the effects of sensory feedback on the generation of different salamander locomotion patterns were investigated.

In this article, we present a novel mathematical model of a CPG. Our model benefits from the advantages of many of the previously published articles. Our model employs a multilayer structure (similar to Refs. [5] and [6]) for better stability and modulability. It also incorporates a number of oscillators (in the form of a Fourier series [13]) to generate sophisticated signal patterns. Oscillators are easy to construct with neuronal structures, and when combined, they are versatile to generate any waveform.

Our CPG model is implemented with a *leaky integrate-and-fire* spiking neuron model, which increases the fidelity of the model. The synaptic weights in the neuron ensembles are calculated using the neural engineering framework (NEF) [14,15]. This method has shown outstanding potential in functional modeling of the brain [14] and motor control system [16]. Additionally, due to the inherent stochasticity of the neuron's behavior, this approach will result in natural variations in the response—a feature that is missing in other deterministic mathematical modeling approaches.

To show the potential of the developed CPG model, it is used to control the periodic motion of a one degree-of-freedom (1DOF) musculoskeletal forearm model [17]. We believe that the same CPG structure, without the need for further development, can be used to generate periodic muscle excitation patterns required in multi-DOF musculoskeletal systems, such as human lower extremities during gait.

To summarize the contributions of this work, we have developed a new multilayer CPG structure, which can generate periodic motions in a musculoskeletal arm model in real-time, and modulate the frequency (speed) of motion using a single descending command. The novel architecture of the CPG model takes advantage of properties of neuronal modeling with the NEF (namely, oscillatory patterns, signal summation, and interpolation), and is

Contributed by the Design Engineering Division of ASME for publication in the Journal of Computational and Nonlinear Dynamics. Manuscript received January 23, 2015; final manuscript received July 7, 2015; published online August 26, 2015. Assoc. Editor: Ahmet S. Yigit.

implemented with spiking neuron models for extra fidelity. Finally, to the best of our knowledge, our CPG model is the only motor control model that can generate humanlike motion variations through a biologically plausible mechanism (i.e., neuronal modeling.)

This article is organized as follows: we first introduce our musculoskeletal forearm model. Then, we present the CPG model structure, which is followed by the details about the implementation with spiking neuron model. The parameter tuning of the CPG model comes next. Finally, results and discussions conclude the paper.

2 Dynamic Modeling

A 1DOF musculoskeletal forearm model is used to highlight the features of our CPG model. The schematic of the forearm model is shown in Fig. 1. As can be seen, the upper arm is assumed to be fixed and the forearm rotates about an ideal revolute joint at the elbow. The forearm is actuated by four muscle groups: brachioradialis (BRD), biceps brachii (BIC), brachialis (BRA), and triceps brachii (TRI). All these muscle groups are flexors, except the TRI group, which is an extensor. This model can capture the important flexion/extension dynamics of the human arm (including muscle dynamics), without introducing unnecessary challenges related to extra DOF.

A Hill-type muscle model is used to describe the muscle behavior in this model (see Appendix A for details). It should be noted that only the contractile element of the Hill muscle model is used in this work. Since the motion in this work is relatively slow, the contribution of tendon dynamics on the system is negligible [18]. Furthermore, including tendons in the model will increase the stiffness of the differential equations, which increases the integration time of the simulation. As will be discussed in Sec. 5, the controller is tuned through a large optimization problem, and a long integration time has significant effect on convergence time of the optimization routine. A model that includes tendon dynamics will still be controllable by the framework presented in this paper, but the optimization time will be much longer (a similar problem that includes tendons is solved in Ref. [17]).

The elbow joint torque, T_e, is calculated from the muscle forces and their moment arms according to

$$T_e = \sum_j F_j r_j \qquad j \in \{\text{BRD}, \text{BIC}, \text{BRA}, \text{TRI}\} \tag{1}$$

where F_j is the muscle force, and r_j is the constant moment arm, which is positive for flexors and negative for extensors. The muscle parameters used in this model are given in Table 1. These parameters are adopted from Ref. [19].

The forearm dynamics can then be written as

$$\ddot{\theta} = \frac{1}{I}\left(T_e - Wd\sin(\theta) - K_d\dot{\theta}\right) \tag{2}$$

The elbow angle, θ, is measured from vertical and is zero when the forearm is fully extended. In Eq. (2), I is the forearm/hand moment of inertia (about elbow joint), and W is the forearm/hand weight, which acts at the distance d from the elbow joint. The damping coefficient ($K_d = 0.2$ N·m s/rad, taken from Ref. [20]) is added to the elbow joint for more stable simulation. The arm mass and inertia properties (Table 2) are calculated using anthropometric data [21] for a 95 kg young Caucasian male.

3 CPG Model

The CPG-based motor control model presented here uses the advantages of two approaches mentioned in the Introduction. This

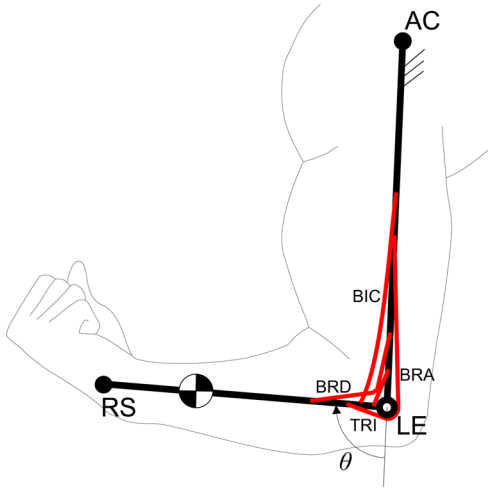

Fig. 1 Schematic of the musculoskeletal forearm model

CPG controller can generate sophisticated muscle activity patterns by a linear combination of oscillators and is modeled in a layered structure.

The framework presented here is applied to the 2D forearm model, and is used to produce a frequency-controllable periodic motion of the elbow flexion/extension, based on a single input. The input to the CPG model resembles the low-dimensional descending command from the higher centers in the CNS, and the output is the high-dimensional motoneuron activities.

The schematic of the CPG controller is shown in Fig. 2. The feedback loops in the figure can be used to modulate the muscle excitation patterns at different levels of the controller. In this work, however, we only focus on the feedforward part of the CPG model.

The CPG model contains a layered structure. The first layer is the pacemaker, which is responsible for generating the *tempo* for muscle activations—how fast each cycle should be. The next layer, the pattern generator, builds continuous and periodic muscle excitation patterns (the *melody*) based on the rhythms of the pacemaker.

3.1 The Pacemaker. The first layer of the CPG controller is the pacemaker. In this model, the pacemaker is in the form of a harmonic oscillator with two states

$$\begin{cases} \dot{x}_1 = \mathcal{D}x_2 \\ \dot{x}_2 = -\mathcal{D}x_1 \end{cases} \tag{3}$$

In this oscillator, $\mathcal{D}$ is the tonic drive (see Fig. 2), which modulates the frequency of oscillations. Increasing the value of the

Table 1 Muscle parameters for the four muscle groups in the 2D forearm model

Parameter	BRD	BIC[a]	BRA	TRI[a]
$F_{0_{\max}}$ (N)	101	855	854	2518
L_0^{CE} (cm)	27	14	10	10
α_p (deg)	5	10	15	15
PCSA (cm^2)	3.08	26	26	76
r^{a} (cm)	3	3.7	5.4	−2

[a]The parameters for these muscles are averaged/summed across different heads of the muscles.
[b]The constant moment arm is the average value over the range of motion.

Table 2 Forearm/hand properties in 2D forearm model

Property	Symbol	Value
Inertia[a]	I	0.152 kg m^2
Weight	W	20.80 N
Center of mass location[a]	d	0.179 m

[a]With respect to elbow joint center.

drive, $\mathcal{D}$, will increase the frequency. The modulation of the frequency of the pacemaker introduces the ability to change the frequency of forearm motion, assuming the pattern generator block can generate proper patterns of muscle excitation.

3.2 The Pattern Generator. The pattern generator builds the required muscle excitation patterns by employing a Fourier series [13,17]. In this work, the fifth-order Fourier series of Eq. (4) is used to generate arbitrary signals with the same period as the principal harmonic of the pacemaker

$$u = \alpha_0 + \sum_{i=1}^{5} \alpha_i \cos(i\mathcal{D}t) + \beta_i \sin(i\mathcal{D}t) \tag{4}$$

Higher harmonics in Eq. (4) can be generated using algebraic functions of the principal harmonic, according to Eqs. (5)–(7)

$$\text{First harmonic}: \begin{cases} \sin(\mathcal{D}t) = x_1 \\ \cos(\mathcal{D}t) = x_2 \end{cases} \tag{5}$$

$$\text{Second harmonic}: \begin{cases} \sin(2\mathcal{D}t) = 2x_1x_2 \\ \cos(2\mathcal{D}t) = 2x_2^2 - 1 \end{cases} \tag{6}$$

$$\text{Third harmonic}: \begin{cases} \sin(3\mathcal{D}t) = 4x_1x_2^2 - x_1 \\ \cos(3\mathcal{D}t) = 4x_2^3 - 3x_2 \end{cases} \tag{7}$$

$$\vdots$$

By changing the tonic drive, the frequency of the pacemaker changes, and if the Fourier coefficients, α_i and β_i, are chosen properly for each muscle, the arm will follow the desired path and with the desired frequency. Thus, it is crucial to use the right Fourier coefficients for each frequency. The tuning of the Fourier parameters is the subject of Sec. 5.

4 Implementation With Spiking Neurons

In the human nervous system, each neuron responds differently to a certain stimulus. Each neuron has a certain threshold beyond which it shows activity. The intensity of the neuron activity will then increase with the intensity of the stimulus. The NEF [14,22] takes advantage of this diversity and calculates the optimal synaptic weight, so that the weighted summation of all neuron activities *decodes* a certain function of the stimulus. The neuron models in the NEF are therefore populated with randomized parameters to span the entire range of stimulus intensities. As an example of this randomized diversity, Fig. 3(*a*) shows the response of 100 neurons to a changing stimulus. In Fig. 3(*b*), the same ensemble of neurons is use to calculate the square of the stimulus intensity, using the synaptic weights found by the NEF. As can be seen in Fig. 3(*b*), due to the inherent noise modeled within each neuron response, the output signal is noisy. This randomness in neuron behavior will result in motion variation, as will be discussed later. For more information about the NEF, the reader is referred to Ref. [22].

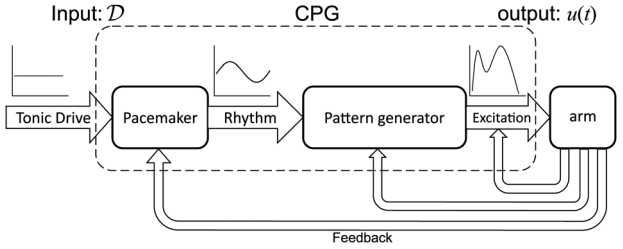

Fig. 2 The layered structure of the CPG controller

Nemo [23] is a MATLAB-based library for NEF and is used to implement the CPG controller with a network of spiking neurons. The two layers of CPG controller are modeled by different ensembles of neurons. The first layer, the pacemaker, is modeled by a two-dimensional ensemble calculating the two oscillating states of Eq. (3)—one dimension for each state, x_1 and x_2. The radius of decoding (the outputs will have the values in this range) for the pacemaker ensemble is 1 for both dimensions. To simulate the oscillations, a feedback projection is used (see Fig. 4). Moreover, as Nemo does not accept arbitrary initial conditions, a step function is used as another projection onto the pacemaker ensemble. This steplike excitation shifts the neurons from their stable state and initializes the oscillations. Thus, the dynamics of the pacemaker ensemble can be summarized as

$$\tau_{ps}\begin{Bmatrix} \dot{x}_1 \\ \dot{x}_2 \end{Bmatrix} = -\begin{Bmatrix} x_1 \\ x_2 \end{Bmatrix} + \overbrace{\begin{bmatrix} 1 & \xi \\ -\xi & 1 \end{bmatrix}\begin{Bmatrix} x_1 \\ x_2 \end{Bmatrix}}^{\text{feedback input}} + \overbrace{\begin{Bmatrix} 1 - \mathcal{H}(t-0.1) \\ 0 \end{Bmatrix}}^{\text{initialization input}} = \begin{Bmatrix} \xi x_2 + 1 - \mathcal{H}(t-0.1) \\ -\xi x_1 \end{Bmatrix} \tag{8}$$

In the above equation, τ_{ps} represents the postsynaptic time constant (the time it takes for the neurons to react to the input stimulation, set equal to 0.01 s). $\mathcal{H}(t-0.1)$ is a Heaviside step function, which allows for the excitation of the oscillator for 0.1 s. Finally, ξ is used to modulate the frequency of oscillation. The relation between ξ and desired frequency, $\mathcal{D}$, is found by trial-and-error to be

$$\xi = 4.76 \times 10^{-2}\mathcal{D} \tag{9}$$

The two states of the pacemaker ensemble represent the principal harmonics of the motion. Higher harmonies are also generated by the pacemaker ensemble, by using origins that decode the relations in Eq. (5).

All five harmonies are decoded in a 10×1 vector and are projected onto four separate pattern generator ensembles to produce the muscle excitation, u, for each muscle group. We have assumed that the motoneuron activities are determined by the overall activity of all the neurons in a pattern generator ensemble. Therefore, the excitation u is determined by the weighted summation of the activities of all the neurons. These synaptic weights are optimally determined by the NEF, so that the output represents the Fourier series (4). The schematic of the connections between the neuron populations is shown in Fig. 4. The termination in each pattern generator ensemble has a transformation vector, $[\mathcal{T}]_{1\times 10}$ containing the Fourier coefficients, that when multiplied by the vector of harmonics will produce the Fourier series of Eq. (4).

The number of neurons in an ensemble is determined by the complexity of the computations it has to perform. The pacemaker

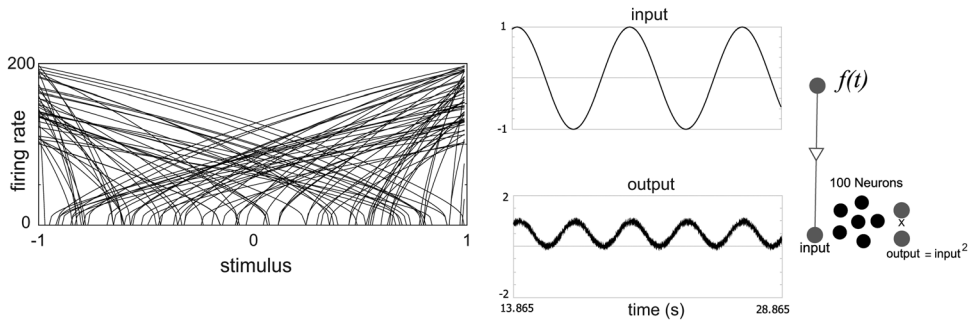

Fig. 3 (*a*) An example for the average firing rate of 100 neurons to a changing stimulus. (*b*) The synaptic weight between the 100 neurons is optimally calculated, so that the weighted sum of the neurons' firing rate represents the square of the input stimulus.

ensemble contains more neurons than the pattern generator ensembles, since it needs to perform a much more complex mathematical calculation. The pacemaker *solves* the differential equations (8) and calculates the nonlinear equations of Eqs. (5)–(7). The pattern generator ensembles, on the other hand, only calculate the linear summation of the inputs (Eq. (4)), which is less computationally demanding and can be handled by a fewer number of neurons. In our simulations, the pacemaker ensemble contains 2000 neurons, while each pattern generator ensemble contains only 200 neurons. Since there are four pattern generator ensembles (one per muscle), there are in total $2000 + 200 \times 4 = 2800$ neurons in this CPG model.

5 Model Parameter Tuning

The desired motion is a periodic flexion/extension of the forearm. The simplicity of this motion allows for more transparent introduction of our CPG model. The elbow angle profile of Fig. 5 is the reference motion, calculated from the average of 20 cycles of the experimental trials. For different frequencies of motion, this profile stretches or shrinks in time.

As mentioned in Sec. 3, because of the nonlinear dynamics of the musculoskeletal system, following the desired forearm motion at different frequencies requires different muscle excitation patterns. This, in turn, means that a different set of Fourier coefficients should be used. Gentle response of the Fourier series to the changes in the Fourier coefficients has been a strong motivation to construct our CPG model in this layered structure. If the proper Fourier coefficients for a number of desired frequencies are known, we can stack them in a look-up table and then interpolate the data to obtain satisfactory coefficients at an arbitrary desired frequency.

To find the proper Fourier coefficients that generate the desired forearm motion at a specific frequency, an optimization problem can be solved. Various criteria have been used as the muscular effort index in the optimizations, including metabolic energy [24,25], muscle force/stress [26–28], and muscle activation/excitation [29,30] (for a review, see Ref. [31]). In a recent study, Sharif Shourijeh and McPhee [17] have shown that the global parameterization approach that minimizes muscle activations results in humanlike muscle activity patterns. Therefore, we have used the same approach to find the Fourier coefficients. Instead of the muscle activations, however, muscle excitation has been used in the cost function. Using the independent variable (i.e., excitations) in the optimization, instead of the dependent states (i.e., activation), improves the convergence time of the optimization routine; due to the fast excitation/activation dynamics, the results will be practically identical. The solution of the optimization problem is, therefore, the set of Fourier coefficients, which generates the muscle excitation patterns required for following the desired motion, at the specified frequency.

In this optimization problem, the Fourier parameters are found, so that the sum of the cost functions (10) and (11) is minimized

$$J_1 = w_1 \frac{1}{T_f} \frac{1}{\sum_j \mathrm{PCSA}_j} \sum_j \left(\mathrm{PCSA}_j \int_0^{T_f} u_j^2 dt \right) \tag{10}$$

$$J_2 = w_2 \frac{1}{T_f} \frac{1}{\theta_{\max}} \int_0^{T_f} (\theta - \theta_{\mathrm{des}})^2 dt \tag{11}$$

In other words

$$\{\alpha_i, \beta_i\} = \arg\min\{J_1 + J_2\} \tag{12}$$

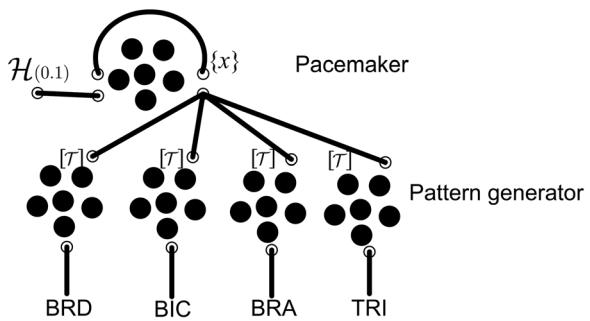

Fig. 4 Schematic of CPG controller implementation with spiking neurons

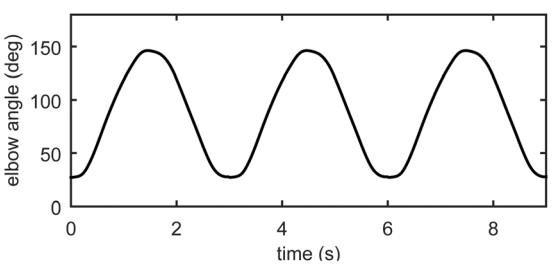

Fig. 5 The reference elbow angle, θ_{des}; three periods of motion are shown

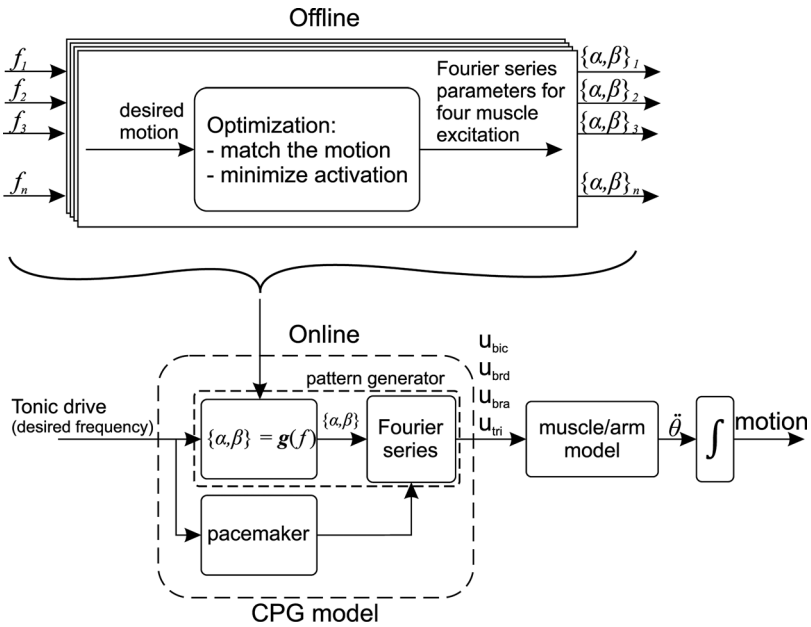

Fig. 6 The optimization framework to find the Fourier series parameters, which will be used in the online generation of muscle excitation signals

subject to the constraints

$$0 \le u_j \le 1 \quad j \in \{\text{BRD}, \text{BIC}, \text{BRA}, \text{TRI}\} \tag{13}$$

In the above relations, J_1 is the physiological effort [17], while J_2 is the tracking error [32]. T_f is the final simulation time, which is chosen to contain a number of cycles of the desired motion. u_j and PCSA_j are muscle excitation and physiological cross section area, respectively, for each muscle group ($j \in \{\text{BRD}, \text{BIC}, \text{BRA}, \textit{TRI}\}$), and θ is the elbow angle that is compared against the desired trajectory, θ_{des}. Finally, w_1 and w_2 are scalar weighting factors calculated as

$$w_1 = 4.5T_{\text{cyc}}^2 \tag{14}$$

$$w_2 = \frac{90}{T_{\text{cyc}}^2} \tag{15}$$

where T_{cyc} is the period of one cycle of the motion. Note that w_1 and w_2 are chosen as the functions of T_{cyc} to balance the relative strength of J_1 and J_2, and to obtain consistent results in terms of motion tracking and efficiency. Slower motions are less intensive, requiring lower muscle excitations. In contrast, the fast motion with high acceleration requires significantly higher excitation levels. Therefore, T_{cyc}^2 is chosen as the measure of the intensity of the motion; slower motion (large T_{cyc}) will reduce the relative importance of tracking and increase the importance of efficiency. Opposite effects are obtained for fast motions, where tracking becomes relatively more important.

For a number of desired frequencies, the corresponding optimization problem is solved offline (see the top part of Fig. 6). Then, these optimal coefficients are stacked in a look-up table. For the fast online control of an arbitrary motion frequency, the data in the look-up table are interpolated to find the Fourier coefficients at the desired frequency. Figure 7 shows the frequency-dependence of the Fourier coefficients for the BRD muscle (numeric data for all muscles are given in Table 3 of Appendix B). These data will be interpolated to find proper coefficients for an arbitrary frequency. Using the interpolated data and the harmonics of the pacemaker, the muscle excitation that generates the desired motion is produced online.

6 Data Collection

To evaluate the model behavior, a subject (24 yr old Caucasian male) performed periodic elbow flexion/extension in the sagittal plane with two speeds: the fast and slow motions, respectively, had periods of $T = 1.5$ s and $T = 3.0$ s. To make sure that the subject performed the motion with the required speed, he was asked to synchronize his motion with a visual cue.

An optical motion tracking system with three active markers (Optotrak Certus, Northern Digital, Inc., Waterloo, ON, Canada) was used to collect the kinematic data. The markers were placed on bony landmarks: acromion (AC), lateral epicondyle (LE), and radial styloid (RS). The elbow angle was then calculated as the angle between the vectors connecting AC to LE and LE to RS (see Fig. 1 for the schematic) as

$$\theta = \arccos\left(\frac{\left(\overrightarrow{\text{LE}-\text{AC}}\right)\cdot\left(\overrightarrow{\text{RS}-\text{LE}}\right)}{\left|\overrightarrow{\text{LE}-\text{AC}}\right|\left|\overrightarrow{\text{RS}-\text{LE}}\right|}\right) \tag{16}$$

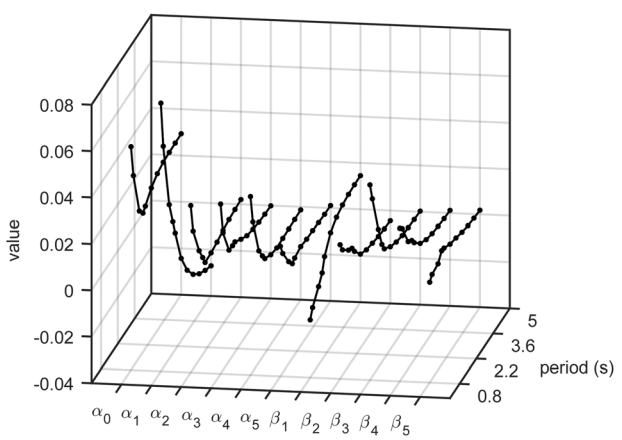

Fig. 7 Optimal Fourier series coefficients for BRD muscle at different periods of motion

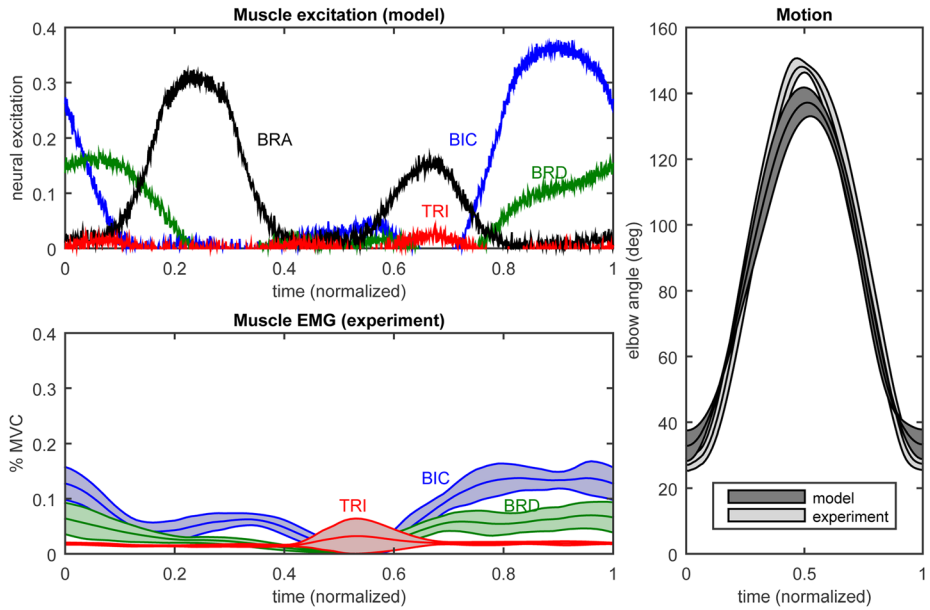

(a)

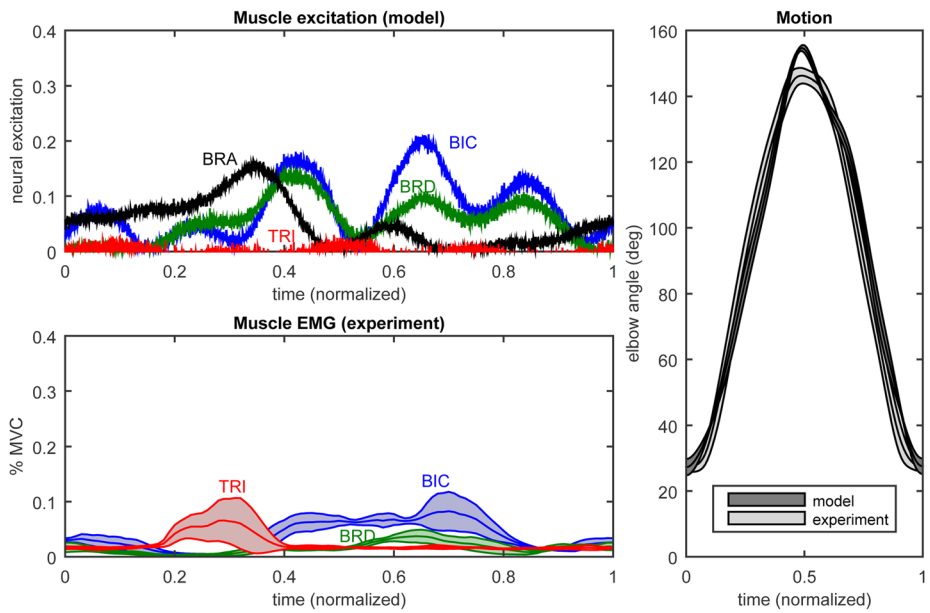

(b)

Fig. 8 Comparison of the experimental data with the CPG model response. Left column compares the muscle excitation patterns in one cycle with the average experimental EMGs. Right column compares the resulting motion between the model and experiments. The results are shown for two speeds of motion: (*a*) fast motion, $T = 1.5$ s and (*b*) slow motion, $T = 3$ s.

Electromyographic (EMG) data from three muscles (BRD, biceps, and long head of triceps) were also collected. BRA is a relatively deep muscle and is difficult to measure by surface EMG electrodes. Thus, no EMG data for this muscle were collected. The EMGs were collected at 4000 Hz, high-pass filtered, full-wave rectified, and then, low-pass filtered (linear envelop) and normalized to the maximum voluntary contraction level.

7 Results

Due to the indeterminacy in neuron behavior, random noise, and decoding error (properties of neural ensembles that are accounted for in the NEF), the output of the neuron ensembles shows variation (notice the noiselike variations in muscle excitation pattern of Fig. 8). Therefore, if the output of the network of neurons is used to drive the musculoskeletal system, the resulting motion will experience variation from one trial to another.

For both the experiment and the simulations, 20 cycles of motion are captured. The duration of each cycle is normalized from 0% to 100% of cycle. Next, the mean and standard deviation of the data are calculated and shown in Fig. 8. The figure compares the model behavior against the experimental data for two different motion frequencies.

The simulation results and the experimental data show similarities. For both the slow and the fast motions, the variation in motion (the standard deviation of motion shown in gray shade in Fig. 8) is similar between the simulation and the experiments. The average motion, although similar, shows slight differences between the simulation and the experiment.

Natural dynamics of the forearm is an important source of the difference in the elbow angle trajectories. The speed of the forearm in a free fall from a flexed position to an extended one under no-activation condition is closer to the speed of the fast motion than the slow motion. Therefore, following the elbow angle trajectory of fast motion is dynamically an easer task. The optimization process makes the compromise between the closeness of the motions and physiological effort, which results in a steeper angle trajectory in the simulation of the slow motion, when compared to that of the fast motion.

The muscle activities (neural excitation levels in the simulation and EMGs in the experiments) have qualitatively similar patterns. However, there are inconsistencies especially in the slower motion (Fig. 8(*b*)). For example, triceps is silent in the simulations, but shows significant EMG activity. One possible explanation for this activity is the role of the long head of triceps in stabilization of the upper arm. In the simulations, the upper arm was assumed to be fixed, but we had asked the subject to hold the upper arm stationary, which requires muscle activity. Other than that, a general agreement can be observed between the muscle excitation patterns in the simulations and EMG patterns in the experimental data.

8 Discussion

The motor control model presented in this article is based on the feedforward aspect of a CPG. The structure of the CPG model allows for easy change in frequency of a rhythmic motion. Since the tuning of the CPG model is based on multiple optimization problems, the output of the motor control model—muscle excitations—are essentially optimal (or close to optimal in interpolated points). Furthermore, since the CPG model interpolates the precalculated optimal data, it can generate the near-optimal muscle excitations very quickly—orders of magnitude faster than solving the optimization problem.

Although this CPG framework has been developed for the control of a 1DOF forearm model, its structure is independent of the motion, the number of muscles, or the DOF. Thus, it is readily applicable to models with more DOF and more muscles. This model is an excellent candidate for the crude control of gait; however, the feedforward nature of this CPG model may result in an unstable response in more complex systems. Thus, to simulate a complex motion such as gait, including feedback loops (shown in Fig. 2) seems to be necessary. The feedback modulation can happen at three stages: at the pacemaker layer (to accelerate or delay the harmonics), at the pattern generator layer (momentarily produce different patterns, e.g., another speed to catch up with a delayed motion), or at the motoneuron level (e.g., monosynaptic reflex loops).

An important contribution of this research is the implementation of the CPG model with spiking neurons. The architecture of the CPG model suits the structure of NEF very well. An oscillator can easily be built by a relatively small number of neurons, and the linear combination of the oscillator outputs is the strength of the NEF approach.

It should be noted that successful implementation of the CPG model with the neurons does not necessarily imply the existence of such a structure in humans; however, it may suggest the possibility of such an architecture in the nervous system for the control of frequency-modulated rhythmic motions. The only tools that were available to us to evaluate our model are at the behavioral level, i.e., the actuator effort (muscle activities) and the resulting motion. The results presented in this paper show that the model is able to replicate the human at the behavior level. Additionally, recent observations at the neuronal level [33] prove the existence of oscillatory neuron activities during arm motion. Putting the pieces together, one may think about the plausibility of the CPG architecture presented here.

The last important feature of the proposed CPG model is its ability to produce a certain level of variation in the resulting motion, similar to the variation in human movements. The source of the variation in our model comes from the inherent stochasticity in the neurons' behavior—the same mechanism as in the human motor control system. This stochasticity results in a realistic *motor noise* which leads to motion variation. To the best of our knowledge, our CPG model is the only published approach that could generate a motion with such variability in a musculoskeletal model and through a biologically plausible methodology.

It should be noted that the model is entirely feedforward. In our human experiments, however, proprioceptive and visual feedback could indeed affect the control performance. Further analysis on the effects of sensory feedback on the control performance of human motion (both in simulation and experiments) is required.

Finally, one specific area that may benefit from motor control models is clinical rehabilitation. It has been shown that employing functional electrical stimulation (FES) during physical therapy can improve the patient's movement scores [34,35]. The current control of FES devices is rudimentary and usually done manually by a therapist. Using fast (real-time) motor control models similar to our CPG model, it is possible to generate muscle activity patterns that can be used to drive the FES device, so that the muscle activities and the resulting motion resemble natural body behavior.

9 Conclusions

In this article, we presented a mathematical model of a motor control system based on the idea of a CPG. We used this model to control rhythmic motion of the forearm. The results showed that our CPG model can produce periodic motion by activating multiple muscles in an optimal way. For this purpose, the CPG model performs a dimensional transformation; it receives a one-dimensional input command (specifying the desired speed of motion) and generates the multidimensional muscle excitation signals. The multilayer structure of the model allows for fast and robust generation of muscle excitation signals and simple frequency control.

The implementation of the CPG model with spiking neurons introduced indeterminacy in the motor control model, which resulted in the same level of motion variation as in the experimental data. The similarity between the simulation results and the experimental data suggests the plausibility of our control mechanism. However, further experimental investigation is necessary to make stronger arguments.

Acknowledgment

The authors would like to thank Dr. Bryan Tripp for his valuable recommendations and providing the source code for Nemo. This project is funded by the Natural Sciences and Engineering Research Council of Canada (NSERC).

Nomenclature

a = muscle activation level
A = corrected activation level in Hill muscle model
A_f = shape factor in Hill muscle model
B = Hill muscle model auxiliary parameter
C = Hill muscle model auxiliary parameter
d = distance from elbow joint to forearm center of mass
$\mathcal{D}$ = tonic drive in CPG model
F = muscle force
$\hat{f}$ = normalized maximum muscle force during elongation

f_l = muscle force–length relation
f_v = muscle force–velocity relation
$F_{0_{\max}}$ = maximum isometric muscle force
$\mathcal{H}$ = Heaviside step function
I = forearm moment of inertia
K_d = damping coefficient at elbow joint
L^{CE} = muscle contractile element length
L_0^{CE} = optimal muscle length
PCSA = muscle physiological cross section area
r = muscle moment arm
$\mathcal{T}$ = presynaptic transformation vector
t_a = muscle activation time constant
t_d = muscle deactivation time constant
t_1 = activation/excitation time constant
t_2 = activation/excitation time constant
T_e = elbow joint torque
T_f = simulation final time
T_{cyc} = period of one cycle of the motion
u = muscle neural excitation
V^{CE} = muscle contractile element shortening velocity
$V_{\max}^{CE}$ = maximum contractile element shortening velocity
w = weighting factor
W = forearm weight
α_i = Fourier series coefficients
α_P = muscle pennation angle
β_i = Fourier series coefficients
γ = shape factor in Hill muscle model
ξ = frequency modulator in CPG model
τ_{ps} = postsynaptic time constant

Appendix A: Muscle Model

Since the interest of this research is in control applications, the muscle model used here is a forward model, i.e., the input of the model is the neural excitation and its output is muscle force. The muscle force is a function of its length and velocity, as well as the activation level [36]. The force–length dependency is given in the following equation:

$$f_l = e^{\left(-\frac{\left(\frac{L^{CE}}{L_0^{CE}}\right)^2}{\gamma}\right)} \tag{A1}$$

In this relation, L^{CE} is the muscle length, L_0^{CE} is the optimal muscle length (at which maximum force can be produced), and γ is a shape factor (assumed to be 0.45).

The force–velocity relation is according to

$$f_v = \begin{cases} \dfrac{V^{CE}}{V_{\max}^{CE} L_0^{CE}} + AV_{\max}^{CE} \\ \dfrac{-V^{CE}}{V_{\max}^{CE} L_0^{CE} A_f} + AV_{\max}^{CE} \end{cases} \quad V^{CE} \le 0$$

$$f_v = \begin{cases} \dfrac{V^{CE} B\hat{f}}{V_{\max}^{CE} L_0^{CE}} + ACV_{\max}^{CE} \\ \dfrac{V^{CE} B}{V_{\max}^{CE} L_0^{CE}} + ACV_{\max}^{CE} \end{cases} \quad V^{CE} > 0 \tag{A2}$$

where A_f is a shape factor, $\hat{f}$ is the normalized maximum muscle force during elongation (adopted to be 1.4), and $V_{\max}^{CE}$ is the normalized maximum muscle velocity (adopted to be 10). A, B, and C are parameters defined below:

$$A = 0.25 + 0.75a \tag{A3}$$

$$B = 2 + \frac{2}{A_f} \tag{A4}$$

$$C = \hat{f} - 1 \tag{A5}$$

In the above relations, a is the muscle activation level, which is calculated from neural excitation, u, according to Ref. [37] as

$$\frac{da}{dt} = (u - a)(t_1 u + t_2) \tag{A6}$$

with t_1 and t_2 defined according to

$$t_2 = \frac{1}{t_d} \tag{A7}$$

$$t_1 = \frac{1}{t_a - t_2} \tag{A8}$$

The activation time constant, t_a, and the deactivation time constant, t_d, are set to 50 and 15 ms, respectively, from Ref. [37].

Knowing the muscle length and the muscle velocity, the muscle force can be calculated according to

$$F = af_l f_v F_{0_{\max}} \cos(\alpha_P) \tag{A9}$$

where $F_{0_{\max}}$ is the maximum isometric muscle force.

Appendix B: Fourier Coefficient Values

Table 3 The optimal Fourier coefficients for the fast and slow motions

	Motion period = 1.5 s				Motion period = 3.0 s			
	BRD	BIC	BRA	TRI	BRD	BIC	BRA	TRI
α_0	0.0465	0.1019	0.0931	0.0020	0.0553	0.0794	0.0507	−0.0027
α_1	0.0756	0.1310	−0.0132	−0.0012	−0.0361	−0.0355	−0.0031	−0.0005
α_2	0.0419	0.0413	−0.0956	0.0013	−0.0084	−0.0007	−0.0078	0.0037
α_3	−0.0075	−0.0311	0.0080	0.0056	−0.0033	0.0097	0.0226	−0.0020
α_4	−0.0132	−0.0089	0.0220	−0.0033	−0.0102	−0.0202	−0.0172	0.0034
α_5	0.0082	0.0092	0.0047	−0.0022	0.0021	0.0048	0.0109	−0.0037
β_1	−0.0013	−0.1019	0.0818	−0.0007	−0.0107	−0.0353	0.0493	0.0013
β_2	0.0028	−0.1106	0.0487	0.0054	−0.0241	−0.0051	−0.0118	0.0037
β_3	0.0105	−0.0576	−0.0597	0.0041	0.0130	0.0270	−0.0004	0.0033
β_4	0.0110	0.0036	−0.0296	−0.0044	−0.0126	−0.0228	0.0081	0.0032
β_5	0.0005	0.0040	0.0253	0.0077	0.0251	0.0539	−0.0092	−0.0018

References

[1] Ijspeert, A. J., 2008, "Central Pattern Generators for Locomotion Control in Animals and Robots: A Review," Neural Networks, **21**(4), pp. 642–653.

[2] MacKay-Lyons, M., 2002, "Central Pattern Generation of Locomotion: A Review of the Evidence," Phys. Ther., **82**(1), pp. 69–83.

[3] Brown, T., 1914, "On the Nature of the Fundamental Activity of the Nervous Centres; Together With an Analysis of the Conditioning of Rhythmic Activity in Progression, and a Theory of the Evolution of Function in the Nervous System," J. Physiol., **48**(1), pp. 18–46.

[4] Noble, J. W., 2010, "Development of a Neuromechanical Model for Investigating Sensorimotor Interactions During Locomotion," Ph.D. thesis, University of Waterloo, ON, Canada.

[5] Rybak, I. A., Shevtsova, N. A., Lafreniere-Roula, M., and McCrea, D. A., 2006, "Modelling Spinal Circuitry Involved in Locomotor Pattern Generation: Insights From Deletions During Fictive Locomotion," J. Physiol., **577**(Pt. 2), pp. 617–639.

[6] Rybak, I. A., Stecina, K., Shevtsova, N. A., and McCrea, D. A., 2006, "Modelling Spinal Circuitry Involved in Locomotor Pattern Generation: Insights From the Effects of Afferent Stimulation," J. Physiol., **577**(Pt. 2), pp. 641–658.

[7] Ekeberg, O., 1993, "A Combined Neuronal and Mechanical Model of Fish Swimming," Biol. Cybern., **69**(5–6), pp. 363–374.

[8] Ekeberg, O., and Grillner, S., 1999, "Simulations of Neuromuscular Control in Lamprey Swimming," Philos. Trans. R. Soc., B, **354**(1385), pp. 895–902.

[9] Kozlov, A., Huss, M., Lansner, A., Kotaleski, J. H., and Grillner, S., 2009, "Simple Cellular and Network Control Principles Govern Complex Patterns of Motor Behavior," Proc. Natl. Acad. Sci. U. S. A., **106**(47), pp. 20027–20032.

[10] Ijspeert, A. J., 2001, "A Connectionist Central Pattern Generator for the Aquatic and Terrestrial Gaits of a Simulated Salamander," Biol. Cybern., **84**(5), pp. 331–348.

[11] Ijspeert, A. J., Crespi, A., Ryczko, D., and Cabelguen, J.-M., 2007, "From Swimming to Walking With a Salamander Robot Driven by a Spinal Cord Model," Science, **315**(5817), pp. 1416–1420.

[12] Harischandra, N., Knuesel, J., Kozlov, A., Bicanski, A., Cabelguen, J.-M., Ijspeert, A. J., and Ekeberg, O., 2011, "Sensory Feedback Plays a Significant Role in Generating Walking Gait and in Gait Transition in Salamanders: A Simulation Study," Front. Neurorobotics, **5**, p. 3.

[13] Sharif Shourijeh, M., and McPhee, J., 2014, "Forward Dynamic Optimization of Human Gait Simulations: A Global Parameterization Approach," ASME J. Comput. Nonlinear Dyn., **9**(3), p. 031018.

[14] Eliasmith, C., Stewart, T. C., Choo, X., Bekolay, T., DeWolf, T., Tang, Y., Tang, C., and Rasmussen, D., 2012, "A Large-Scale Model of the Functioning Brain," Science, **338**(6111), pp. 1202–1205.

[15] Eliasmith, C., 2013, *How to Build a Brain: A Neural Architecture for Biological Cognition*, Oxford University Press, New York.

[16] DeWolf, T., and Eliasmith, C., 2011, "The Neural Optimal Control Hierarchy for Motor Control," J. Neural Eng., **8**(6), p. 065009.

[17] Sharif Shourijeh, M., and McPhee, J., 2013, "Optimal Control and Forward Dynamics of Human Periodic Motions Using Fourier Series for Muscle Excitation Patterns," ASME J. Comput. Nonlinear Dyn., **9**(2), p. 021005.

[18] Silva, M. P. T., and Ambrósio, J. A. C., 2003, "Solution of Redundant Muscle Forces in Human Locomotion With Multibody Dynamics and Optimization Tools," Mech. Based Des. Struct. Mach., **31**(3), pp. 381–411.

[19] Garner, B. A., and Pandy, M. G., 2001, "Musculoskeletal Model of the Upper Limb Based on the Visible Human Male Dataset," Comput. Methods Biomech. Biomed. Eng., **4**(2), pp. 37–41.

[20] Lebiedowska, M. K., 2006, "Dynamic Properties of Human Limb Segments," *International Encyclopedia of Ergonomics and Human Factors*, 2nd ed., Vol. 3, W. Karwowski, ed., CRC Press, London, p. 137.

[21] Leva, P. D., 1996, "Adjustments to Zatsiorsky–Seluyanov's Segment Inertia Parameters," J. Biomech., **29**(9), pp. 1223–1230.

[22] Eliasmith, C., and Anderson, C. H., 2003, *Neural Engineering Computation, Representation, and Dynamics in Neurobiological Systems*, MIT Press, Cambridge, MA.

[23] Tripp, B., 2014, "Software—Bryan Tripp," accessed Dec. 4, 2014, http://bptripp.com/node/3

[24] Anderson, F. C., and Pandy, M. G., 2001, "Dynamic Optimization of Human Walking," ASME J. Biomech. Eng., **123**(5), pp. 381–390.

[25] Anderson, F. C., and Pandy, M. G., 2001, "Static and Dynamic Optimization Solutions for Gait Are Practically Equivalent," J. Biomech., **34**(2), pp. 153–161.

[26] An, K.-N., Kwak, B. M., Chao, E. Y., and Morrey, B. F., 1984, "Determination of Muscle and Joint Forces: A New Technique to Solve the Indeterminate Problem," ASME J. Biomech. Eng., **106**(4), pp. 364–367.

[27] Happee, R., and Van der Helm, F. C. T., 1995, "The Control of Shoulder Muscles During Goal Directed Movements, an Inverse Dynamic Analysis," J. Biomech., **28**(10), pp. 1179–1191.

[28] Prilutsky, B. I., and Zatsiorsky, V. M., 2002, "Optimization-Based Models of Muscle Coordination," Exercise Sport Sci. Rev., **30**(1), pp. 32–38.

[29] Thelen, D. G., and Anderson, F. C., 2006, "Using Computed Muscle Control to Generate Forward Dynamic Simulations of Human Walking From Experimental Data," J. Biomech., **39**(6), pp. 1107–1115.

[30] Ackermann, M., and van den Bogert, A. J., 2010, "Optimality Principles for Model-Based Prediction of Human Gait," J. Biomech., **43**(6), pp. 1055–1060.

[31] Erdemir, A., McLean, S., Herzog, W., and van den Bogert, A. J., 2007, "Model-Based Estimation of Muscle Forces Exerted During Movements," Clin. Biomech., **22**(2), pp. 131–154.

[32] Mehrabi, N., Sharif Razavian, R., and McPhee, J., 2015, "A Physics-Based Musculoskeletal Driver Model to Study Steering Tasks," ASME J. Comput. Nonlinear Dyn., **10**(2), pp. 1–8.

[33] Churchland, M. M., Cunningham, J. P., Kaufman, M. T., Foster, J. D., Nuyujukian, P., Ryu, S. I., and Shenoy, K. V., 2012, "Neural Population Dynamics During Reaching," Nature, **487**(7405), pp. 51–56.

[34] Thrasher, T. A., Zivanovic, V., McIlroy, W., and Popovic, M. R., 2008, "Rehabilitation of Reaching and Grasping Function in Severe Hemiplegic Patients Using Functional Electrical Stimulation Therapy," Neurorehabilitation Neural Repair, **22**(6), pp. 706–714.

[35] Kapadia, N. M., Nagai, M. K., Zivanovic, V., Bernstein, J., Woodhouse, J., Rumney, P., and Popovic, M. R., 2013, "Functional Electrical Stimulation Therapy for Recovery of Reaching and Grasping in Severe Chronic Pediatric Stroke Patients," J. Child Neurol., **29**(4), pp. 1–7.

[36] Thelen, D. G., 2003, "Adjustment of Muscle Mechanics Model Parameters to Simulate Dynamic Contractions in Older Adults," ASME J. Biomech. Eng., **125**(1), pp. 70–77.

[37] Winters, J. M., and Stark, L., 1988, "Estimated Mechanical Properties of Synergistic Muscles Involved in Movements of a Variety of Human Joints," J. Biomech., **21**(12), pp. 1027–1041.